# Extraction of Kaon Formfactors from $K^- \to \mu^- \nu \gamma$ Decay at ISTRA+ Setup

V. A. Duk *, V. N. Bolotov, V. A. Lebedev, A. A. Khudyakov,
A. I. Makarov, A. Yu. Polyarush, V. P. Novikov
*Institute for Nuclear Research of RAS, Moscow, Russia*
S. A. Akimenko, G. I. Britvich, A. P. Filin, A. V. Inyakin,
I. Ya. Korolkov, V. M. Leontiev, V. F. Obraztsov, V. A. Polyakov,
V. I. Romanovsky, O. G. Tchikilev, V. A. Uvarov, O. P. Yushchenko
*Institute for High Energy Physics, Protvino, Russia*

**Abstract**

The radiative decay $K^- \to \mu^- \nu_\mu \gamma$ has been studied at ISTRA+ setup in a new kinematical region. About 46K events of $K^- \to \mu^- \nu_\mu \gamma$ have been observed. The sign and value of $F_V - F_A$ have been measured for the first time. The result is $F_V - F_A = 0.16 \pm 0.04(stat) \pm 0.05(syst)$.

## 1 Introduction

Radiative kaon decays are dominated by long distance (low energy) physics. For low energy processes there are no direct predictions from SM and effective theories such as Chiral pertubation theory ($\chi$PT) are used. $\chi$PT gives quantitative predictions for most kaon decay modes. That is why radiative kaon decays provide a testing ground for $\chi$PT. Moreover, these decays are sensitive to New Physics.

The decay $K^- \to \mu^- \nu_\mu \gamma$ is sensitive to hadronic weak currents in low-energy region. The decay amplitude includes two terms: internal bremsstrahlung (IB) and structure dependent term (SD). IB contains radiative corrections from $K^- \to \mu^- \nu_\mu$. SD allows to probe electroweak structure of kaon.

The differential decay rate can be written in terms of standard kinematical variables x=$2E^\star_\gamma/M_k$ and $y = 2E^\star_\mu/M_k$ (see [1] for details), $E^\star_\gamma$ being photon energy and $E^\star_\mu$ muon energy in cms. It includes IB, $SD^\pm$ parts and their interference $INT^\pm$. The $SD^\pm$ and $INT^\pm$ contributions are determined by two formfactors $F_V$ and $F_A$.

The general formula for decay rate is as follows:

$$\frac{d\Gamma}{dxdy} = A_{IB} f_{IB}(x,y) + A_{SD}[(F_V + F_A)^2 f_{SD^+}(x,y) + (F_V - F_A)^2 f_{SD^-}(x,y)]$$

$$-A_{INT}[(F_V + F_A) f_{INT^+}(x,y) + (F_V - F_A) f_{INT^-}(x,y)]$$

where

$$f_{IB}(x,y) = [\tfrac{1-y+r}{x^2(x+y-1-r)}][x^2 + 2(1-x)(1-r) - \tfrac{2xr(1-r)}{x+y-1-r}],$$

$$f_{SD^+}(x,y) = [x + y - 1 - r][(x+y-1)(1-x) - r],$$

* **e-mail**:Viacheslav.Duk@cern.ch

$f_{SD^-}(x,y) = [1-y+r][(1-x)(1-y)+r]$,

$f_{INT^+}(x,y) = [\frac{1-y+r}{x(x+y-1-r)}][x^2-(1-x)(1-x-y)+r]$,

$f_{INT^-}(x,y) = [\frac{1-y+r}{x(x+y-1-r)}][x^2-(1-x)(1-x-y)-r]$,

and $r = (\frac{M_\mu}{M_K})^2$, $A_{IB} = \Gamma_{K_{\mu 2}} \frac{\alpha}{2\pi} \frac{1}{(1-r)^2}$, $A_{SD} = \Gamma_{K_{\mu 2}} \frac{\alpha}{8\pi} \frac{1}{r(1-r)^2} [\frac{M_K}{F_K}]^2$, $A_{INT} = \Gamma_{K_{\mu 2}} \frac{\alpha}{2\pi} \frac{1}{(1-r)^2} \frac{M_K}{F_K}$. In these formulae, $\alpha$ is the fine structure constant, $F_K$ is $K^+$ decay constant ($F_K = 155.5 \pm 0.2 \pm 0.8 \pm 0.2 MeV$ [2]), and $\Gamma_{K_{\mu 2}}$ is $K_{\mu 2}$ decay width. Distributions on dalitz-plot for different terms are shown in fig. 1÷4.

$F_V \pm F_A$ are calculated within $\chi$PT ($O(p^4)$ [1], $O(p^6)$ [3]) and LFQM model [4]. In general, $F_V$ and $F_A$ depend on $q^2 = (P_K - P_\gamma)^2 = M_K^2(1-x)$. In the $O(p^4)$ $\chi$PT they are constant and $F_V + F_A = 0.137$, $F_V - F_A = 0.052$. We will initially assume $F_V$ and $F_A$ constant and then test for their dependence on $q^2$.

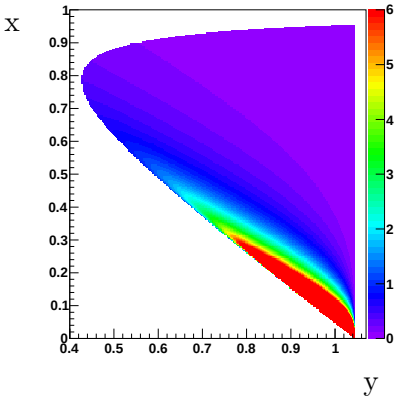


Figure 1: IB

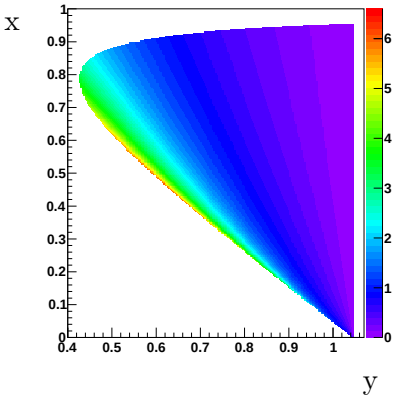


Figure 2: INT-

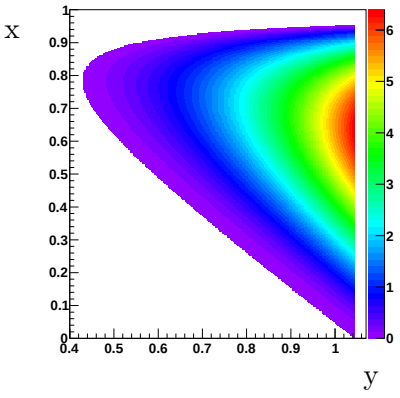


Figure 3: SD+

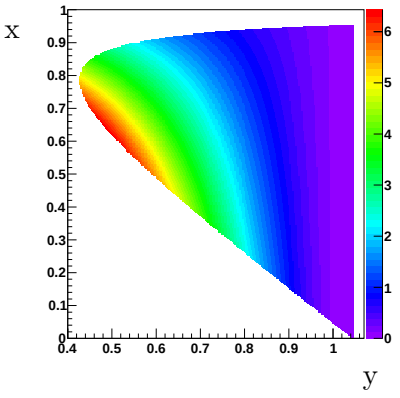


Figure 4: *SD-*

Experimentally, the decay $K^- \to \mu^- \nu_\mu \gamma$ was studied mostly in the IB dominated region (see [5],[6],[7]). There was only one formfactor measurement in E787 experiment [8]. In this study, SD+ term was extracted and $|F_V + F_A|$ was obtained to be $|F_V + F_A| = 0.165 \pm 0.007(stat) \pm 0.011(syst)$. Also $F_V - F_A$ was constrained: $-0.04 < F_V - F_A < 0.24$. $F_V - F_A$ was measured by E865 experiment in $K \to \mu\nu e^+ e^-$ decay [9]: $F_V - F_A = 0.077 \pm 0.028$. The goal of our study is to measure $K \to \mu\nu\gamma$ decay in the kinematical region where INT- term (and hence $F_V - F_A$) can be extracted.

# 2 Experimental setup

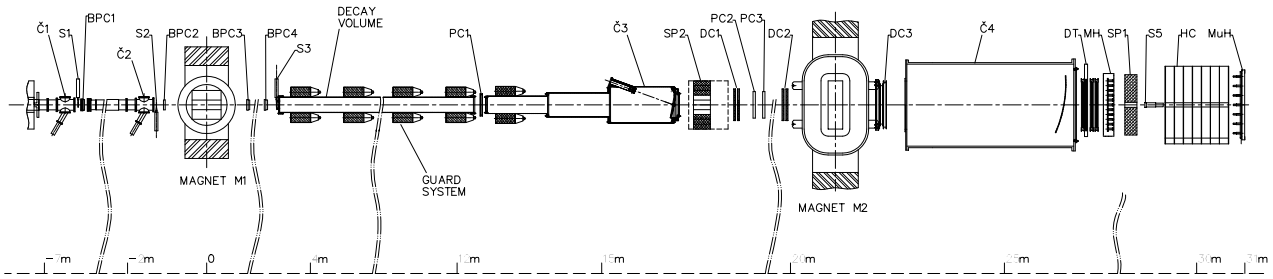


Figure 5: Elevation view of the ISTRA+ detector.

The experiment was performed at the IHEP 70 GeV proton synchrotron U-70. The experimental setup ISTRA+ (fig. 5) was described in some details elsewhere[10]. The setup was located in the negative unseparated secondary beam. The beam momentum in the measurements was $\sim$ 26 GeV with $\Delta p/p \sim 1.5\%$. The admixture of $K^-$ in the beam was $\sim 3\%$. The beam intensity was $\sim 3 \cdot 10^6$ per 1.9 sec U-70 spill. The beam particle deflected by $M_1$ was detected by $BPC_1 \div BPC_4$ (1mm step multiwire chambers), the kaon identification was done by $\check{C}_0 \div \check{C}_2$ threshold $\check{C}$-counters. A 9 meter long vacuum decay volume was surrounded by 8 lead glass rings $LG_1 \div LG_8$ used to veto low energy photons. $SP_2$ was a lead glass calorimeter to detect/veto large angle photons. The decay products deflected in M2 with 1Tm field integral were measured by $PC_1 \div PC_3$ (2mm step proportional chambers); $DC_1 \div DC_3$ (1cm cell drift chambers) and finally by 2cm diameter drift tubes $DT_1 \div DT_4$. Wide aperture threshold Cerenkov counters $\check{C}_3$, $\check{C}_4$ were filled with He and were not used in the measurements. Nevertheless $\check{C}_3$ was used as the extension of the decay volume. $SP_1$ (ECAL) was a 576-cell lead glass calorimeter, followed by HC - a scintillator-iron sampling hadron calorimeter. HC was subdivided into 7 longitudinal sections 7×7 cells each. MH was a 11×11 cell scintillating hodoscope used to improve the time resolution of the tracking system, MuH was a 7×7 cell muon hodoscope.

The trigger was provided by $S_1 \div S_5$ scintillation counters, $\check{C}_0 \div \check{C}_2$ Cerenkov counters, analog sum of amplitudes from the last dinodes of the $SP_1$ : $T_0 = S_1 \cdot S_2 \cdot S_3 \cdot \bar{S}_4 \cdot \check{C}_0 \cdot \bar{\check{C}}_1 \cdot \bar{\check{C}}_2 \cdot \bar{S}_5 \cdot \Sigma(SP_1)$, here $S_4$ was a scintillator counter with a hole to suppress beam halo ; $S_5$ was a counter downstream the setup at the beam focus; $\Sigma(SP_1)$- a requirement for the analog sum of ECAL amplitudes to be above $\sim$3 GeV. The last requirement served to suppress the $K \to \mu\nu$ decay. About $\sim 10\%$ events were recorded with a different trigger: $T_1 = S_1 \cdot S_2 \cdot S_3 \cdot \bar{S}_4 \cdot \check{C}_0 \cdot \bar{\check{C}}_1 \cdot \bar{\check{C}}_2 \cdot \bar{S}_5$. This prescaled trigger allowed to calculate trigger effiency as a function of the energy released in ECAL.

# 3 Event selection

## 3.1 Selection criteria and general cuts

The decay is identified as follows: one primary track (kaon), one negatively charged secondary track, $\mu$ flag in HCAL; one shower in ECAL not associated with the charged track. Muon identification using HCAL is described in our previous papers ([11],[12]).

Several cuts are applied to clean the data:

- number of beam and decay tracks in both X and Y projections is equal to 1;

- CL of primary tracks in both X and Y projections must be greater than $10^{-2}$;
- CL of decay tracks is greater than 0.1 (decay-X) and 0.15 (decay-Y);
- the angle between primary (kaon) and secondary (muon) track is greater than 2 mrad.

The last cut eliminates most undecayed beam particles. The quality of decay track (described quantitavely by CL) is worse than that of beam track because of multiple scattering and detector resolution.

Cuts containing photon energy include:
- Gamma energy in kaon rest frame is greater than 10 MeV;
- no photons in SP2 calorimeter (energy threshold is 0.5 GeV for total energy release);
- no photons in GS.

For vertex characteristics we have the following requirements:
- z-coordinate must be within the interval $400 < z < 1600$cm;
- $(-3) < x_{vtx} < 3$cm;
- $(-2) < y_{vtx} < 6$cm;
- CL of general vertex fit is greater than $10^{-2}$.

Additional cuts are applied to suppress backgrounds:
- number of hits in matrix hodoscope (MH) is less than 3;
- missing momentum does not point to the ECAL central hole (this cut effectively rejects K$\pi$2 background since missing particle is the lost photon in this case);

### 3.2 Trigger efficiency

As $T_0$ trigger described in Section 2 contains energy threshold in SP1 the trigger efficiency as a function of energy released in ECAL should be found using events with $T_1$ trigger: $\epsilon_{trg} = (T_1 \bigcap T_0)\ /\ T_1$. Trigger curve is shown in the fig. 6. The fit is done using Fermi function. For the further analysis only events with $T_0$ are kept and these events are weighted by the factor of $1/\epsilon_{trg}$.

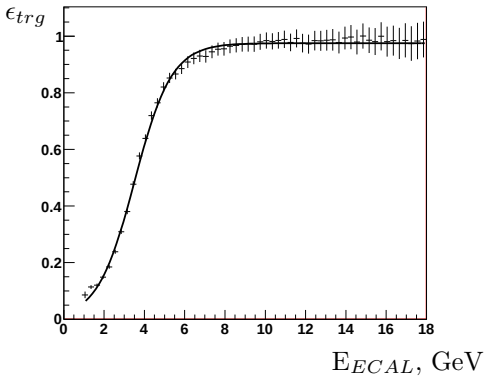


Figure 6: $T_0$ trigger efficiency

## 4 Signal extraction

Distribution over M($\mu\nu\gamma$) is used for signal observation. $M^2(\mu\nu\gamma) = (P_\mu + P_\nu + P_\gamma)^2$ where $P_\mu, P_\nu, P_\gamma$ are 4-momenta of corresponding particles; missing mass $m_\nu$ is supposed to be equal to 0 so that $\overrightarrow{p}_\nu = \overrightarrow{p}_K - \overrightarrow{p}_\mu - \overrightarrow{p}_\gamma; E_\nu = |\overrightarrow{p}_\nu|$. M($\mu\nu\gamma$) peaks at $K^-$ mass for the signal. Main background comes from 2 decay modes: $K^- \to \mu^-\nu\pi^0 (K\mu 3)$ and $K^- \to \pi^-\pi^0 (K\pi 2)$ with one

gamma lost from $\pi^0 \to \gamma\gamma$ and $\pi$ misidentified as $\mu$. Distributions on dalits-plot for $K\mu 3$ and $K\pi 2$ are shown in fig. 7, 8.

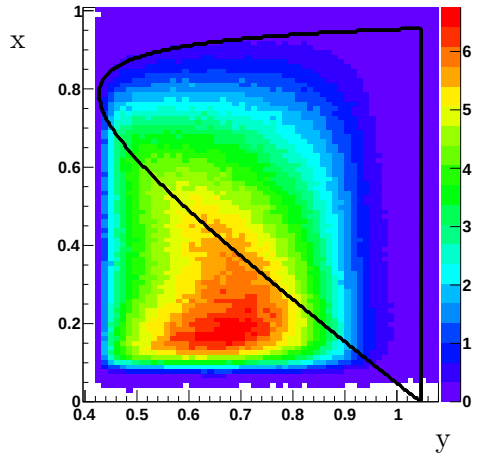


Figure 7: *Dalitz-plot density for $K\mu 3$ background*

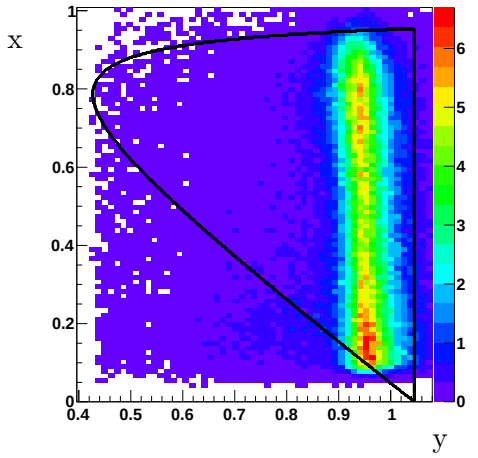


Figure 8: *Dalitz-plot density for $K\pi 2$ background*

### 4.1 Signal extraction procedure

The procedure starts with dividing all kinematical (x,y) region into stripes on x (x-stripes). The stripe width is $\Delta$x=0.05 ($\Delta E^*_\gamma \sim 24 MeV$). In every x-stripe we put a cut on y: $y_{min} < y < y_{max}$. $y_{min}$ and $y_{max}$ are selected from the maximization of signal significance defined as $\frac{S}{\sqrt{S+B}}$

Besides distributions over M($\mu\nu\gamma$) and y, we use cos $\theta^*_{\mu\gamma}$ for the signal extraction, $\theta^*_{\mu\gamma}$ being the angle between $\vec{p}_\mu$ and $\vec{p}_\gamma$ in c.m.s. We put a cut on cos $\theta^*_{\mu\gamma}$ to reject background in those stripes where distributions over cos $\theta^*_{\mu\gamma}$ for signal and background differ a lot.

Finally for each x-stripe we obtain events with cuts on y and cos $\theta^*_{\mu\gamma}$. Now we construct M($\mu\nu\gamma$) which will be used for the fit. Fitting M($\mu\nu\gamma$) alone is not sufficient because in some stripes distributions for signal and background are very similar. Also it would be difficult to distinguish between two backgrounds - K$\mu$3 and K$\pi$2. That is why we take three histograms (y; cos $\theta^*_{\mu\gamma}$ with cut on y; M($\mu\nu\gamma$) with cuts on y and cos $\theta^*_{\mu\gamma}$) and fit them simultaneously. Both signal and background shapes are taken from MC. MC histograms are smoothed and the result is written as a function. The simultaneous fit gives us signal event number in each x-stripe.

As we use the same data several times we should take care about correct estimation of statistical error:

- do simultaneous fit of three histograms and obtain $\{p_i\}$ - best parameter values (they correspond to global $\chi^2$ minimum);

- take $\{p_i\}$ as initial values and perform $\chi^2$/ndf and error estimation for one histogram M($\mu\nu\gamma$) using MINOS program.

### 4.2 Selected kinematical region

For further analysis we have selected eleven x-stripes in the following region: $0.05 < x < 0.6$ ($13 MeV < E^\star_\gamma < 150 MeV$). Last stripe is used in systematics study only (see Sec.5 and 6). Cuts on y and cos $\theta^*_{\mu\gamma}$ are summarized in table.1.

The y-width changes from stripe to stripe, in average $\Delta y \sim 0.2$. Our kinematical region is sensitive to INT- term (fig. 9) and complementary to that of previous experiments [8],[5] (fig. 10). Stripe borders are slightly out of allowed kinematical region because of resolution.

| strip | cut on x | cut on y | $\Delta$y | cut on cos $\theta^*_{\mu\gamma}$ |
|---|---|---|---|---|
| 01 | $0.05 < x < 0.1$ | 0.9÷1.1 | 0.2 | $> -0.8$ |
| 02 | $0.1 < x < 0.15$ | 0.9÷1.1 | 0.2 | $> -0.8$ |
| 03 | $0.15 < x < 0.2$ | 0.85÷1. | 0.15 | $> -0.8$ |
| 04 | $0.2 < x < 0.25$ | 0.8÷0.95 | 0.15 | $> -0.2$ |
| 05 | $0.25 < x < 0.3$ | 0.75÷0.9 | 0.15 | $> -0.3$ |
| 06 | $0.3 < x < 0.35$ | 0.72÷0.87 | 0.15 | $> -0.4$ |
| 07 | $0.35 < x < 0.4$ | 0.65÷0.85 | 0.2 | $> -0.3$ |
| 08 | $0.4 < x < 0.45$ | 0.62÷0.85 | 0.23 | $> -0.5$ |
| 09 | $0.45 < x < 0.5$ | 0.57÷0.8 | 0.23 | $> -0.7$ |
| 10 | $0.5 < x < 0.55$ | 0.52÷0.75 | 0.23 | – |
| 11 | $0.55 < x < 0.6$ | 0.48÷0.7 | 0.22 | – |

Table 1: Cuts on y and cos $\theta^*_{\mu\gamma}$ in x-stripes

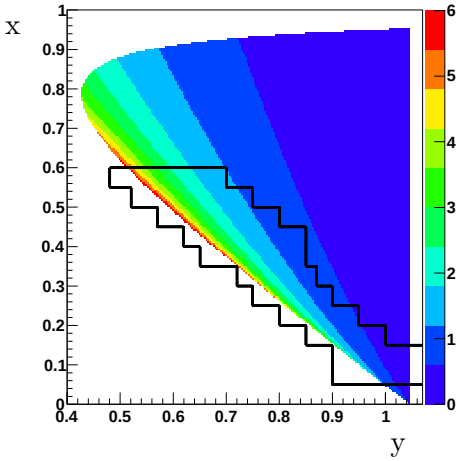


Figure 9: *INT- dalitz-plot density and selected kinematical region*

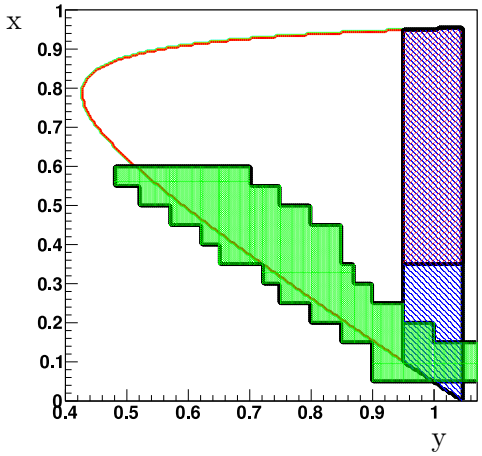


Figure 10: *$x$=$2E^\star_\gamma/M_k$, $y = 2E^\star_\mu/M_k$ ISTRA+(green); BNL E787(red hatch); KEK-104(blue hatch)*

Results of simultaneous fit for stripes #2 ($0.1 < x < 0.15$) and #9 ($0.45 < x < 0.5$) are shown in fig. 11, 12. The total event number is 46194.

## 5 $F_V - F_A$ measurement

For each x-stripe we have experimental event number $N_{exp}$ from fitting the data and IB event number $N_{IB}$ from MC (see fig. 13). Then we plot $N_{exp}/N_{IB}$ as a function of x where each bin corresponds to a certain x-stripe (see fig. 14).

For IB only we would have $N_{exp}/N_{IB} \approx 1$. It is the case for small x where IB is dominated and INT- is negligible. For large x we see that $N_{exp}$ also contains negative interference term. We fit $N_{exp}/N_{IB}$ distribution with $(f_{IB}(x) - f_{INT-}(x,p))/f_{IB}(x)$ where fit parameter p corresponds to $F_V - F_A$ ($F_V$ and $F_A$ are initially assumed to be constant). The result of the final fit is as follows: $F_V - F_A = 0.16 \pm 0.04(stat)$. Number of 'missing events' due to negative INT$^-$ term is 1969 which is $\sim 4\%$ of expected IB contribution (48163 events). It should be noted that the last stripe is not included in the fit. In this stripe background is very large and signal can be easily misidentified as background during simultaneous fit. Nevertheless we will use this stripe for systematics study (see Sec.6).

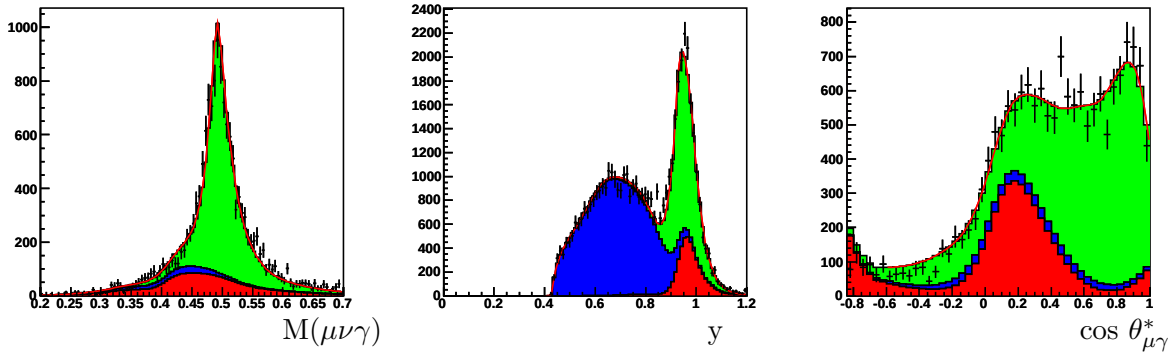


Figure 11: Simultaneous fit in stripe 2: M($\mu\nu\gamma$), y and cos $\theta^*_{\mu\gamma}$. Points with errors - data, blue - $K\mu3$, red - $K\pi2$, green - signal, red line - signal+background. $\chi^2$/ndf=111.5/95 (for mass histogram only, see text).

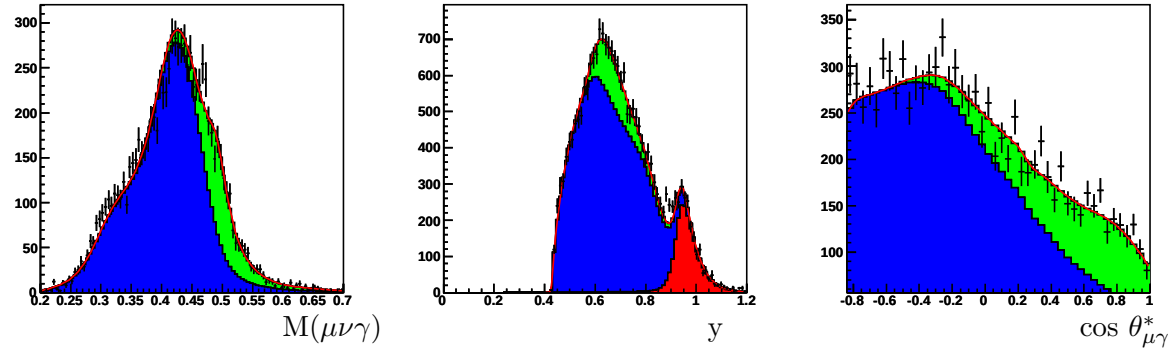


Figure 12: Simultaneous fit in stripe 9: M($\mu\nu\gamma$), y and cos $\theta^*_{\mu\gamma}$. Points with errors - data, blue - $K\mu3$, red - $K\pi2$, green - signal, red line - signal+background. $\chi^2$/ndf=140.0/100 (for mass histogram only, see text).

## 6 Systematic error estimation

The main potential sources of systematic error are:
- possible wrong choice of signal/background shape in the simultaneous fit;
- cut on x (i.e. number of x-stripes);
- cut on y in x-stripes;
- cut on z-coordinate of the vertex.

Each source is investigated separately and errors are considered to be independent.

**Possible wrong choice of signal/background shape in the simultaneous fit**. For estimation of shape systematics we scale errors in each bin of the final fit (each bin corresponds to a certain x-stripe) proportional to $\sqrt{\chi^2}$ where $\chi^2$ is obtained in the simultaneous fit for the bin. Then we repeat final fit. New value of $F_V - F_A$ is consistent with the main one and the fit error is larger: $\sigma_{fit} \sim 5.3 \times 10^{-2}$. We treat $\sigma_{fit}$ as follows: $\sigma_{fit} = \sqrt{\sigma^2_{stat} + \sigma^2_{syst,fit}}$ with $\sigma_{syst,fit}$ being systematical error caused by non-ideal shape of signal and background distributions: $\sigma_{syst,fit} \sim 3.2 \times 10^{-2}$.

**Cut on x**. Each x-stripe has the width $\Delta x$=0.05. By adding/removing stripes involved in the fit on the left(right) border and repeating final fit with the new cut on x we can see how

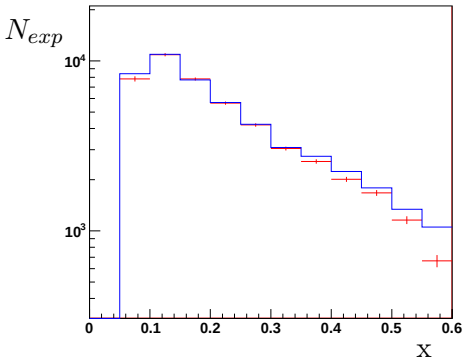


Figure 13: *x-spectrum. Red points - data, blue histogram - IB*

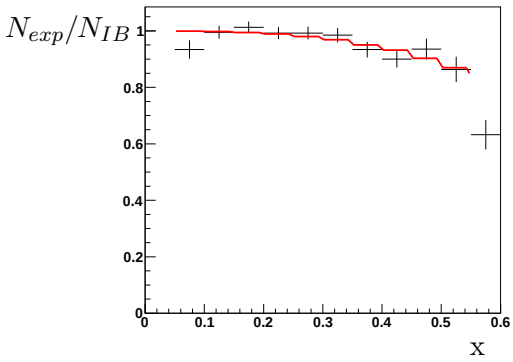


Figure 14: $N_{exp}/N_{IB}$ *for x-stripes and final fit.* $\chi^2/ndf$*=7.7/8*

$F_V - F_A$ depends on the x-cut value. For the left border, we take results of 3 fits which include stripes 1÷10(main fit), 2÷10 and 3÷10. For the right border, we choose fits including stripes 1÷9, 1÷10(main fit), 1÷11.

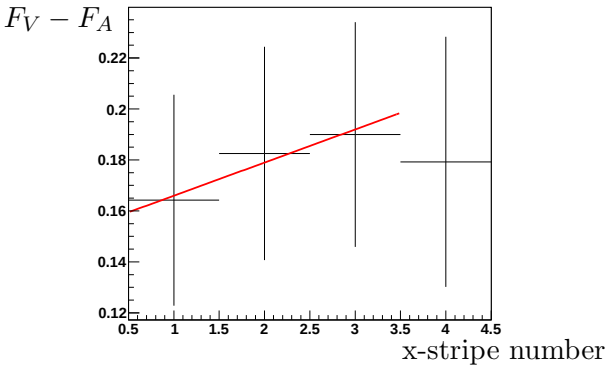


Figure 15: *Systematics of cut on x. Left border*

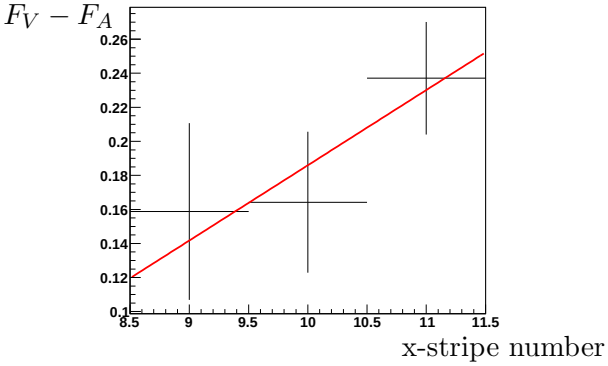


Figure 16: *Systematics of cut on x. Right border*

The resulting plots $F_V - F_A$ vs x-cut are shown in fig. 15 and 16 It is seen that except 1÷11 fit the values $F_V - F_A$ are stable. That is why we do not use stripe 11 in the main fit. For the conservative estimate of systematics we nevertheless fit these plots with straight lines. The line slope multiplied by the resolution in x (which is taken from MC) gives systematic error of this cut. The systematic error of the right border is found to be $\sim 3.1 \times 10^{-2}$ and that of the left border is negligible.

**Cut on y in x-stripes**. To investigate this source of systematics we choose cut on y in a different way. Instead of using significance we take distribution over y for signal MC in a certain x-stripe and select events inside FWHM. Such cuts on y are stronger than those made using significance. We redo simultaneous fit in x-stripes and final fit. The obtained result is consistent with the main one. No systematics is found here.

**Cut on z-coordinate of the vertex**. To study this systematics we divided events into two groups - with $z < 1100cm$ and $z > 1100cm$. The events with $z < 1100cm$ use PC1 in the decay track reconstruction while events with $z > 1100cm$ do not. Besides that the second group of events has the vertex inside the decay volume filled with He. It could be a possible source of systematics. Repeating the whole procedure (simultaneous fit in x-stripes and final fit) we obtain two values for $F_V - F_A$ which are averaged. To get $\chi^2$ equal to one, we have to scale statistical errors by the factor of $\sqrt{\chi^2}$. The additional error is treated as systematic one and

equals to $\sim 2.3 \times 10^{-2}$.

**Total systematic error**. Now we quadratically sum all sources supposing the errors to be independent and obtain $\epsilon_{syst} \sim 5.0 \times 10^{-2}$.

# 7 Final result

With this estimation of systematic error we finally get our result: $F_V - F_A = 0.16 \pm 0.04(stat) \pm 0.05(syst)$. It is $\sim 1.7\sigma$ larger than theoretical prediction within $\chi$PT at O($p^4$) and consistent with experimental result [9].

The $O(p^6)$ $\chi PT$ gives linear dependence of $F_V$ and $F_A$ on $q^2$ (see [3]) and hence on x. We use $F_V$ and $F_A$ parametrization given in [13]: $F_V = F_V(0)\ [1 + \lambda(1 - x)]$, $F_A$=const. This theoretical prediction was tested in three ways. First, we take both $F_V$ and $F_A$ from $O(p^6)$ $\chi PT$ ($F_V(0) = 0.082$, $F_A$=0.034, $\lambda$=0.4) and do the final fit. $\chi^2$ of this fit is 13.4/9 ($\sim 1\sigma$ from $\chi^2 = 1$). Second, we take $F_V(0)$ and $F_A$ from $O(p^6)$ $\chi PT$ and take $\lambda$ as a fit parameter. It gives $\lambda = 2.7 \pm 1.0(stat) \pm 1.3(syst)$ with $\chi^2$=8.03/8 (fig. 17). And finally we fix $F_V(0)$ from $O(p^6)$ $\chi PT$ and take $\lambda$ and $F_A$ as fit parameters. Correlation between them is shown in fig. 19. Theoretical prediction is slightly out of $2\sigma$-ellipse (fig. 20).

In LFQM, $F_V$ and $F_A$ depend on $q^2$ in a complicated way (see [4]). Final fit is shown in fig. 18. LFQM is disfavoured ($\sim 1.6\sigma$ from $\chi^2 = 1$) although can not be excluded.

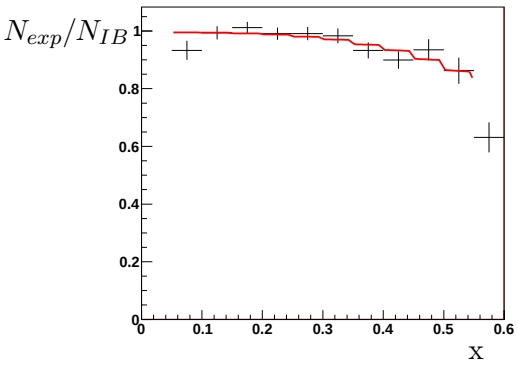


Figure 17: *$\chi PT$ $O(p^6)$ fit, $F_V(0)$ and $F_A$ taken from theory. $\chi^2$/ndf=8.03/8*

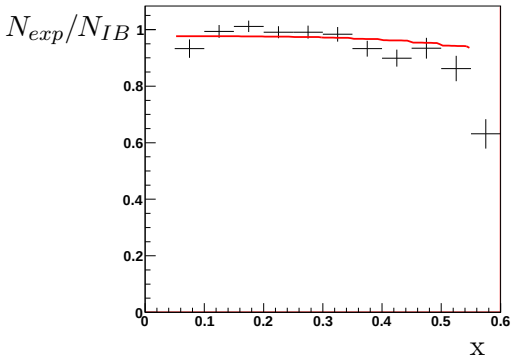


Figure 18: *LFQM fit. $\chi^2$/ndf=15.8/9*

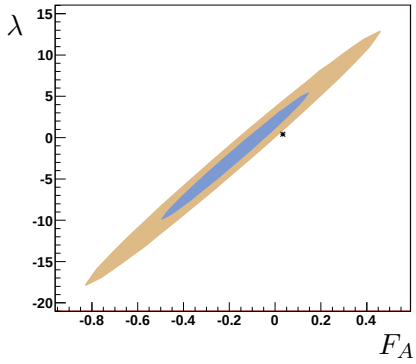


Figure 19: *$\chi PT$ $O(p^6)$ fit, $F_V(0)$ taken from theory. $\chi^2/ndf = 7.6/7$*

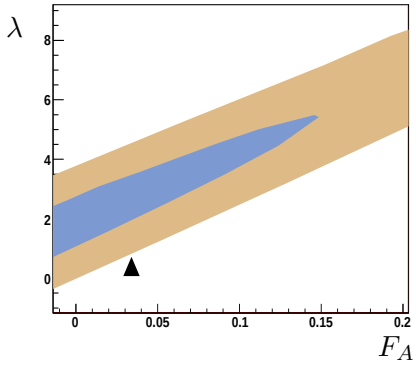


Figure 20: *$\chi PT$ $O(p^6)$ fit, $F_V(0)$ taken from theory. $\chi^2/ndf = 7.6/7$*

## 8 Conclusions

The radiative decay $K^- \to \mu^- \nu_\mu \gamma$ has been studied using in-flight decays at ISTRA+ setup. About 46K events of $K^- \to \mu^- \nu_\mu \gamma$ (it is the largest statistics for this decay) have been found in a new kinematical region. The negative $INT^-$ term has been observed and as a result $F_V - F_A$ has been measured: $F_V - F_A = 0.16 \pm 0.04(stat) \pm 0.05(syst)$. The result is $\sim 1.7\sigma$ above $O(p^4)$ $\chi$PT prediction.

An alternative analysis done by our collaboration is presented in [14]. The results are compatible.

Authors would like to thank C.Q. Geng and E. Goudzovsky for the code plotting formfactors in LFQM. The work is supported by Russian Foundation for Basic Research (grant 07-02-00957).

## References

[1] J.Bijnens, G.Ecker and J.Gasser, Nucl.Phys. B396, 81 (1993); J.Bijnens et al., "Semileptonic kaon decays", 2nd DAPHNE Physics Handbook, 315 (1994).

[2] C.Amsler et al. Particle Data Group. Phys.Lett.B667 (2008) 1.

[3] C.Q.Geng et al. Nucl.Phys. B684 (2004) 281-317; hep-ph/0306165.

[4] Chuan-Hung Chen et al. Phys.Rev.D77:014004,2008; hep-ph/0710.2971.

[5] Y.Akiba et al. Phys.Rev.D32:2911,1985.

[6] V.S.Demidov et al. Sov.J.Nucl.Phys.52:1006-1011,1990, Yad.Fiz.52:1595-1604,1990.

[7] V.V.Barmin et al. Sov.J.Nucl.Phys.47:643,1988, Yad.Fiz.47:1011-1014,1988.

[8] S.C.Adler et al. Phys.Rev.Lett.85:2256-2259,2000; hep-ex/0003019.

[9] A.A.Poblaguev et al. Phys.Rev.Lett.89(2002) 061803.

[10] V.N.Bolotov et al. IHEP preprint 8-98,1998.

[11] I.V.Ajinenko et al. Phys.Atom.Nucl. 66(2003) 105; Yad.Fiz. 66 (2003) 107.

[12] O.P.Yushchenko et al. Phys.Lett. B581 (2004) 31.

[13] F.Ambrosino et al. Eur. Phys. J. C64 (2009) 627.

[14] O.Tchikilev et al. IHEP-2008-27, Jan 2010. 15pp. hep-ex/1001.0374.